JHEP

Published for SISSA by Springer

Received: June 23, 2014
Revised: December 11, 2014
Accepted: January 10, 2015
Published: January 27, 2015

Medium-induced soft gluon radiation in forward dijet production in relativistic proton-nucleus collisions

Stéphane Peigné[a] **and Rodion Kolevatov**[a,b]

[a] *SUBATECH, UMR 6457, Université de Nantes, Ecole des Mines de Nantes, IN2P3/CNRS, 4 rue Alfred Kastler, 44307 Nantes cedex 3, France*

[b] *Department of High Energy Physics, Saint-Petersburg State University, Ulyanovskaya 1, 198504, Saint-Petersburg, Russia*

E-mail: peigne@subatech.in2p3.fr, kolevato@subatech.in2p3.fr

Abstract: Considering forward dijet production in the $q \to qg$ partonic process, we derive the spectrum of accompanying soft gluon radiation induced by rescatterings in a nuclear target. The spectrum is obtained to logarithmic accuracy for an arbitrary energy sharing between the final quark and gluon, and for final transverse momenta as well as momentum imbalance being large as compared to transverse momentum nuclear broadening. In the case of equal energy sharing and for approximately back-to-back quark and gluon transverse momenta, we reproduce a previous result of Liou and Mueller. Interpreting our result, we conjecture a simple formula for the medium-induced radiation spectrum associated to hard forward $1 \to n$ processes, which we explicitly check in the case of the $g \to gg$ process.

Keywords: QCD Phenomenology

ArXiv ePrint: 1405.4241

doi:10.1007/JHEP01(2015)141

Contents

1 Introduction and summary

The phenomenological importance of medium-induced gluon radiation associated to the production of high-$p_\perp$ hadrons in collisions involving relativistic nuclei has been established about two decades ago. Various approaches using different setups (projectile type, specific observable, kinematical range, etc.) have been explored, as well as their applications to the description of experimentally observed phenomena. In particular, medium-induced parton energy loss in a hot quark-gluon plasma was found to provide a natural explanation of the suppression of high-$p_\perp$ hadron spectra in high-energy nucleus-nucleus collisions (see ref. [1] for an overview and references therein).

Comparatively, medium-induced radiation in the collision of a light projectile (hadron or electron) with a nuclear target (in which collision one does not a priori expect the formation of the quark-gluon plasma), received much less attention. Still, the importance of induced gluon radiation also in this situation and especially for particle production at moderate $p_\perp$ and forward rapidity has been recognized by several authors. For example, the effects due to initial and final state radiation in hadron and Drell-Yan production at forward rapidity in p–A (or d–A) collisions have been studied, in particular in refs. [2–4].

On the other hand, a few years ago the role of the coherent radiation arising from the interference between emission amplitudes off the incoming and outgoing particles was emphasized [5]. Such interferences are expected in all situations where the hard partonic process in the nuclear target rest frame is effectively equivalent to the forward scattering of an incoming parton to an outgoing compact *colored* system of partons. Moreover, the interference can come into play only when the phase space for gluon radiation with large enough formation time t_f is available, i.e., when the energy of the effective color charge

JHEP01(2015)141

crossing the medium is large enough. In ref. [5], the medium-induced radiation off an energetic gluon crossing a nuclear medium was studied in the specific kinematics where the gluon energy E (in the medium rest frame) is *asymptotically* large, $E \to \infty$, the other (transverse momentum) scales of the problem being fixed. In this kinematical setup, which we will also choose in the present study (see below and section 2.1 for more details), the average medium-induced energy loss ΔE turns out to scale as E, and the behavior $\Delta E \propto E$ arises from soft gluon radiation with formation time $t_{\rm f}$ also scaling as E, thus being *fully coherent* over the medium size ($t_{\rm f} \gg L$, with L the fixed medium size) at asymptotically large E [5]. It is important to point out that the behavior $\Delta E \propto E$ also arises when E is not too large, namely in the Gunion-Bertsch incoherent radiation limit where the typical radiation formation time does not exceed the mean free path of the energetic parton in the medium. Such behavior was also found in refs. [2, 3] for initial-state medium-induced bremsstrahlung.

Fully coherent energy loss should play an important role in high-energy *hadro*production of hadrons, but should be absent in (inclusive) Drell-Yan production, as well as in hadron photoproduction. In the case of J/ψ hadroproduction at low $p_\perp \lesssim M_{{\rm J}/\psi}$, viewed in the target rest frame as the scattering of an incoming gluon to an outgoing *color octet* compact $c\bar{c}$ pair, such energy loss was shown to provide a successful description of J/ψ nuclear suppression in proton-nucleus (p–A) as compared to proton-proton (p–p) collisions, from fixed-target (SPS, HERA, FNAL) to collider (RHIC, LHC) energies [6–8].

Before studying the possible effect of coherent energy loss on other observables, one should first consider the question of the process dependence of the medium-induced coherent radiation spectrum $\omega {\rm d}I/{\rm d}\omega$. Recent studies [9, 10] started to address this question. The radiation spectra associated to $1 \to 1$ [10] and $1 \to 2$ [9] forward scattering processes are found to be proportional to the same logarithm of the kinematical parameters, but to possibly differ by an overall factor. For instance, Liou and Mueller showed that the $q \to qg$ and $g \to q\bar{q}$ processes, in the kinematics where the outgoing jets have identical longitudinal momenta and nearly back-to-back transverse momenta, lead to the same medium-induced radiation spectrum up to a surprising factor 4/5 [9].

In the present study, we derive the coherent radiation spectrum associated to the $q \to qg$ process already studied in [9], but using slightly more general kinematics. First, we consider the outgoing gluon and quark to carry the fractions $x_{\rm h}$ and $(1-x_{\rm h})$ of the incoming (light-cone) longitudinal momentum p^+ ($x_{\rm h} = 1/2$ was chosen in [9]). Second, not only the final gluon and quark transverse momenta $\vec{K}_{1\perp} \equiv \boldsymbol{K}_1$ and $\vec{K}_{2\perp} \equiv \boldsymbol{K}_2$, *but also their momentum imbalance* $\boldsymbol{K}_1 + \boldsymbol{K}_2 \equiv \boldsymbol{q}$, are chosen to be hard compared to the transverse momentum broadening $\Delta q_\perp$ across the medium, $|\boldsymbol{K}_1|, |\boldsymbol{K}_2|, |\boldsymbol{q}| \gg \Delta q_\perp$. However, similarly to [9] (and also to [5, 10]), we focus on the specific asymptotic limit already mentioned above, namely $p^+ \to \infty$ at fixed $|\boldsymbol{K}_1|$, $|\boldsymbol{q}|$ and $|\Delta q_\perp|$. Within this setup, the radiation spectrum associated to $q \to qg$ is derived in the opacity expansion (as in [10] for $1 \to 1$ forward processes), and in the large N_c limit (as in [9]). Throughout our calculation we are using the (physical) light-cone $A^+ = 0$ gauge[1] with polarization vectors of the radiated

[1] We limit our calculation to the light-cone gauge, as in ref. [9]. For an example of an explicit calculation of medium-induced radiation in different gauges, see ref. [11].

JHEP01(2015)141

gluon satisfying $\epsilon^+(k) = 0$, $\epsilon^-(k) = 2\,\vec{\epsilon}_\perp \cdot \vec{k}_\perp/k^+$ and $\sum \epsilon_\perp^{\mu\,*}\epsilon_\perp^\nu = -g_\perp^{\mu\nu}$ for the sum over the two physical polarization states. The resulting radiation spectrum is proportional to the same leading logarithm as in refs. [9, 10], but with a prefactor depending on the hard $q \to qg$ process through the kinematical variables $x_{\rm h}$, $\boldsymbol{q}$, $\boldsymbol{K}_1$. This prefactor is simply interpreted as the probability for the qg pair to be produced in the $\bar{\mathbf{6}} \oplus \mathbf{15}$ subspace of all possible qg color states. For $|\boldsymbol{q}| \ll |\boldsymbol{K}_1|$ and $x_{\rm h} = 1/2$ we recover the factor 4/5 found in [9]. We conjecture a simple formula (3.27) for the medium-induced radiation spectrum associated to hard forward $1 \to n$ processes. The conjecture is explicitly verified in the case of the $g \to gg$ process, where in the particular limit $|\boldsymbol{q}| \ll |\boldsymbol{K}_1|$ and $x_{\rm h} = 1/2$ we find the overall factor 5/3, instead of 4/5 for the $q \to qg$ process.

In section 2 we review the theoretical setup and the results of refs. [5, 10] for $1 \to 1$ forward processes, and give a physical interpretation of the main features of the medium-induced coherent radiation spectrum. The setup and calculation are generalized to the hard $q \to qg$ and $g \to gg$ processes in section 3. In the final section 4, we briefly discuss the link between our study and the phenomenology of nuclear suppression in p–A collisions.

2 Forward single jet production

2.1 Review of previous studies

Consider a massless parton of large momentum $p = (p^+, 0, \vec{0}_\perp)$ with $p^+ \equiv 2E$,[2] prepared in the far past and traversing some nuclear medium, see figure 1. The final energetic 'jet' is 'tagged' with a transverse momentum $\boldsymbol{p}'$ much larger than the nuclear transverse broadening $\boldsymbol{\ell} = \sum \boldsymbol{\ell}_i$ acquired through multiple *soft* scattering. As a consequence $\boldsymbol{p}'$ must arise dominantly from a *single hard* scattering $\boldsymbol{q} \simeq \boldsymbol{p}'$, with $|\boldsymbol{q}| \gg |\boldsymbol{\ell}|$. We focus on the $p^+ \to \infty$ limit at fixed transverse momentum (small angle scattering). The fast parton is also assumed to scatter with a negligible longitudinal momentum transfer to the medium, which allows one to neglect the recoil of the target partons. This setup is used in [5, 10] to derive the medium-induced coherent radiation associated to 'forward single jet' production (i.e., $1 \to 1$ forward production), which we briefly review below. In the following, the radiated gluon momentum is denoted by $k = (k^+, \boldsymbol{k}^2/k^+, \boldsymbol{k} \equiv \vec{k}_\perp)$, and we focus on soft ($x \equiv k^+/p^+ \ll 1$) and small angle ($|\boldsymbol{k}| \ll k^+$) radiation (hence $k^+ \equiv \omega + k^z \simeq 2\omega$). As we will see, the main features of coherent radiation induced by $1 \to 1$ processes also arise for the $1 \to 2$ process ($q \to qg$) studied in section 3. This is because coherent radiation, in the limit considered in section 3, effectively sees the 'dijet' qg final state as a pointlike object.

In this work we define the intensity of soft radiation accompanying the hard production of some final state with specific kinematics (characterized by the hard momentum p') by the ratio:

$$\mathrm{d}I = \frac{\mathrm{d}\sigma_{\rm rad}(p', k)}{\mathrm{d}\sigma_{\rm prod}(p')}\,. \tag{2.1}$$

Here the denominator represents the inclusive cross section for producing the final state under consideration, while the numerator is the inclusive cross section for producing the

[2] We use light-cone variables, $p = (p^+, p^-, \boldsymbol{p})$, with $p^\pm = p^0 \pm p^z$ and $\boldsymbol{p} \equiv \vec{p}_\perp$.

JHEP01(2015)141

final state *and* a soft gluon. Formally the latter, integrated over the radiated gluon phase space, enters the denominator as one of the contributions. However, to leading order in α_s, the denominator can be approximated by the hard production cross section *without* soft gluon emission. Moreover, assuming that soft rescatterings of the leading parton do not affect $\mathrm{d}\sigma_{\mathrm{prod}}(p')$, the latter can be calculated as if there were no rescattering in the medium, i.e., at zeroth order in the opacity expansion [12].

On the contrary, the numerator of (2.1) is modified by soft rescatterings and must be represented as an expansion in the number n of scattering centers encountered by the leading parton. The $n = 0$ term in this expansion coincides with the radiation cross section in absence of a medium, and thus cancels out in the *medium-induced* radiation intensity defined as

$$\mathrm{d}I^{\mathrm{induced}} \equiv \mathrm{d}I - \mathrm{d}I^{\mathrm{vacuum}} = \sum_{n=1}^{\infty} \frac{\mathrm{d}\sigma_{\mathrm{rad}}^{(n)}(p',k)}{\mathrm{d}\sigma_{\mathrm{prod}}(p')} \equiv \sum_{n=1}^{\infty} \mathrm{d}I^{(n)} \,. \tag{2.2}$$

The definition of the induced spectrum as it stands in (2.1) represents the conditional probability of having gluon radiation provided a given final state *with specific kinematics* is produced in a hard process. In particular, when several hard subprocesses are possible (in the case of di-jet production the subprocesses may differ by the color representation of the final state), (2.1) reduces to the sum of induced spectra for each of the subprocesses, weighted by the corresponding subprocess probability. As we will briefly argue in section 4, for the interpretation of the accompanying radiation spectrum in terms of induced energy loss, the spectrum should be considered for each channel separately. However, in the following sections we calculate the quantity defined by (2.1) and (2.2), which will allow a comparison of our result with that of ref. [9] where the same definition was used.

In ref. [5] the medium-induced coherent radiation spectrum $\mathrm{d}I/\mathrm{d}x$ associated to the $g \to g$ process (with the final 'gluon' being a compact color octet $Q\bar{Q}$ pair of mass M) was derived by modeling the transverse momentum broadening $\Delta q_\perp$ across the medium by a *single* rescattering $\ell_\perp$, and identifying $\ell_\perp^2 = \Delta q_\perp^2(L) = \hat{q}L$, where $\hat{q} = \mu^2/\lambda_g$, with μ the typical transverse momentum exchange in a single scattering and λ_g the gluon mean free path in the medium. The obtained result,

$$x\frac{\mathrm{d}I}{\mathrm{d}x}\bigg|_{g\to g} = N_c \frac{\alpha_s}{\pi} \log\left(1 + \frac{\Delta q_\perp^2(L)}{x^2 M_\perp^2}\right), \tag{2.3}$$

where $M_\perp^2 \equiv M^2 + p_\perp'^2 \simeq M^2 + q_\perp^2$, was confirmed in [10] in a theoretical setup using the opacity expansion [12], allowing one to consider an arbitrary number n of soft rescatterings in the medium.

More precisely, it was shown in ref. [10] that at small enough x, (2.3) has the same *parametric* behavior (in particular as a function of L) as the exact spectrum, provided $\Delta q_\perp^2(L)$ is defined as the *typical* transverse broadening. In the case of a Coulomb scattering potential considered in [10] and in the present study, the latter reads $\Delta q_\perp^2(L) \simeq \hat{q}L \log L/\lambda_g$ at very large L (specifically, when $\log L/\lambda_g \gg 1$), see for instance ref. [13]. However, using $\Delta q_\perp^2(L) = \hat{q}L \log L/\lambda_g$ in (2.3), the expression (2.3) turns out to be *numerically* a very accurate approximation to the exact spectrum as soon as $\log L/\lambda_g \geq 1$, and up to

JHEP01(2015)141

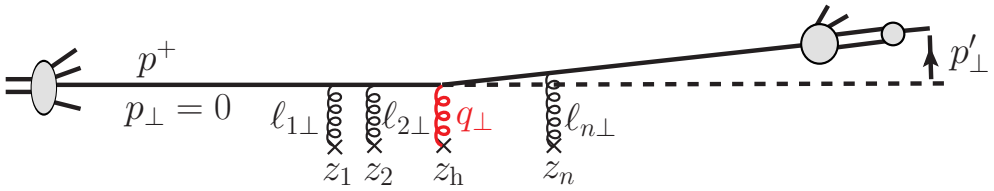

Figure 1. Setup for $1 \to 1$ forward production used in [5, 10], as viewed in the nuclear target rest frame. The solid line denotes the energetic parton (gluon or quark). The hard process is modeled by a transverse momentum exchange $q_\perp$ (in red) occurring at the longitudinal position z_h, and supplemented by soft rescatterings $\ell_{i\perp} \ll q_\perp$ (with also $\ell_\perp = |\sum \boldsymbol{\ell}_i| \ll q_\perp$) occurring at longitudinal positions z_i.

values of $x \sim \Delta q_\perp(L)/M_\perp$ [10]. Thus, for both parametric and numerical accuracy, we set $\Delta q_\perp^2(L) = \hat{q} L \log L/\lambda_g$ (rather than simply $\hat{q}L$) in (2.3) and in the following.

In the present paper we focus on the case of massless particles and, similarly to ref. [9], on the small-x region where the spectrum is logarithmically enhanced. We thus rewrite (2.3) as

$$x\frac{\mathrm{d}I}{\mathrm{d}x}\bigg|_{g\to g} = N_c\,\frac{\alpha_s}{\pi}\left[\log\left(\frac{\Delta q_\perp^2(L)}{x^2 q_\perp^2}\right) + \mathcal{O}(1)\right]. \tag{2.4}$$

We stress that the latter expression holds when not only the argument of the logarithm, but the logarithm itself is much larger than unity, i.e., to *logarithmic accuracy*, which will be implicit throughout our study.[3]

It is useful to recall the basic steps leading to (2.4). It was shown in [10] that the spectrum at order n in the opacity expansion is given by

$$x\frac{\mathrm{d}I^{(n)}}{\mathrm{d}x} = \frac{\alpha_s}{\pi^2}\int \mathrm{d}^2\boldsymbol{k}\left[\prod_{i=1}^{n}\int\frac{\mathrm{d}z_i}{C_R\lambda_R}\int \mathrm{d}^2\boldsymbol{\ell}_i\, V(\boldsymbol{\ell}_i)\right] \frac{\sum}{}$$

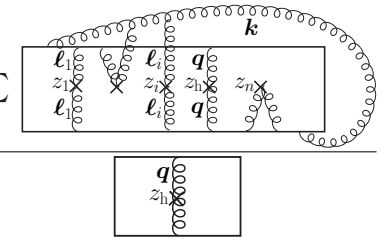

(2.5)

where the diagrams appearing in the numerator and denominator are evaluated using the pictorial rules defined in figure 2. The upper (lower) part of each diagram appearing in the numerator of (2.5) corresponds to a contribution to the emission amplitude (conjugate amplitude) of the soft gluon $\boldsymbol{k}$ induced by the rescatterings $\boldsymbol{\ell}_i$. The diagram in the denominator stands for the hard process 'cross section' (which here is a single color factor, other factors cancelling between numerator and denominator). The quantity λ_R is the elastic mean free path of the fast parton of color charge C_R (note that the product

[3] It might seem that within logarithmic accuracy, the factor $\log L/\lambda_g$ in the expression of the typical broadening $\Delta q_\perp^2(L) = \hat{q} L \log L/\lambda_g$ should be irrelevant, since $\log\log L/\lambda_g$ is realistically $\sim \mathcal{O}(1)$. However, this amounts to consider the small x limit of (2.4) at fixed L. As explained in the former paragraph, setting $\Delta q_\perp^2(L) = \hat{q} L \log L/\lambda_g$ allows the spectrum (2.4) to have a correct L dependence (at fixed x), both parametrically and numerically.

JHEP01(2015)141

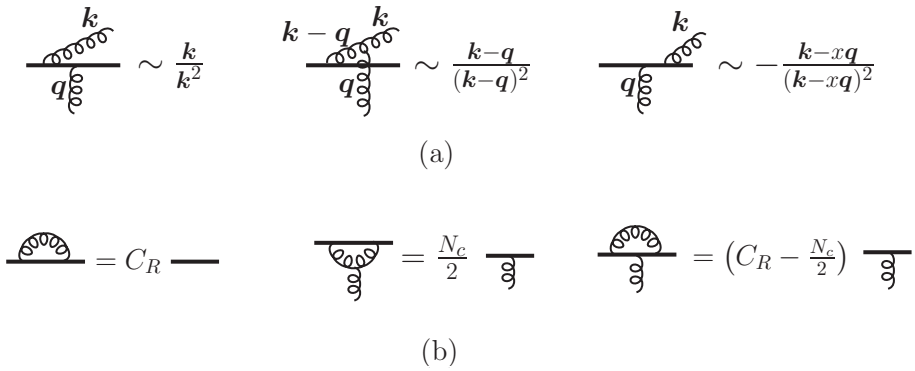

Figure 2. Pictorial rules for (a) emission vertices and (b) color factors. The energetic parton of color charge C_R is denoted by the solid line ($C_R = C_A = N_c$ for a gluon and $C_R = C_F = (N_c^2-1)/(2N_c)$ for a quark). For the pictorial representation of color factors, see for instance ref. [14].

$C_R\lambda_R = C_F\lambda_q = N_c\lambda_g$ is independent of the parton type), and an average over soft transfers $\boldsymbol{\ell}_i$ is performed using the screened Coulomb potential $V(\boldsymbol{\ell}_i) = \mu^2/[\pi(\boldsymbol{\ell}_i^2+\mu^2)^2]$. The latter provides the typical magnitude of soft transfers, $|\boldsymbol{\ell}_i| \sim \mu \ll |\boldsymbol{q}|$, with μ being the inverse screening length of the medium.

We stress that the evaluation of (2.5) in [10] is done in the limits $t_{\rm f} \gg L$ and $k_\perp \ll q_\perp$ (which can be justified a posteriori, see below), which leads to important simplifications:

(i) The diagrams where the time t associated to the soft emission vertex is in between two rescatterings, $z_i < t < z_{i+1}$, are proportional to the difference $\sim (e^{i\varphi_{i+1}} - e^{i\varphi_i})$ between two 'phase factors', where $\varphi_i \propto z_i/t_{\rm f}$ [15], and vanish in the limit $t_{\rm f} \gg L$.

(ii) The diagrams where the hard gluon exchange $\boldsymbol{q}$ couples to the soft radiated gluon $\boldsymbol{k}$ are suppressed as $\boldsymbol{k}^2/\boldsymbol{q}^2$ due to the hard momentum $\boldsymbol{q}$ entering the soft gluon propagator. However the rescattering gluons $\boldsymbol{\ell}_i$ can couple to both the energetic parton and the soft gluon, including virtual contributions where two gluon lines $\boldsymbol{\ell}_i$ and $-\boldsymbol{\ell}_i$ are transferred in either the amplitude or conjugate amplitude.

(iii) At each order in opacity, and to leading logarithmic accuracy (as defined after (2.4)) considered throughout our study, the contribution to (2.5) of purely initial state radiation can easily be checked to be negligible. (The same holds for purely final state radiation.) Only interference diagrams remain, like the generic diagram drawn in the numerator of (2.5).

At first order in opacity we find [10]

$$x\frac{\mathrm{d}I^{(1)}}{\mathrm{d}x} = (2C_R - N_c)\,\frac{\alpha_s}{\pi^2}\,\frac{L}{\lambda_g}\int \mathrm{d}^2\boldsymbol{k}\int \mathrm{d}^2\boldsymbol{\ell}_1\, V(\boldsymbol{\ell}_1)\left[\frac{\boldsymbol{k}-\boldsymbol{\ell}_1}{(\boldsymbol{k}-\boldsymbol{\ell}_1)^2} - \frac{\boldsymbol{k}}{\boldsymbol{k}^2}\right]\cdot\frac{-(\boldsymbol{k}-x\boldsymbol{q})}{(\boldsymbol{k}-x\boldsymbol{q})^2}\,, \quad (2.6)$$

which can be interpreted as the interference between the wavefunction of the final parton-gluon fluctuation (the last factor in the integrand of (2.6)), and the incoming 'medium-induced wavefunction' (factor in between brackets). For the purpose of the present study, it

JHEP01(2015)141

is sufficient to observe that when $x|\boldsymbol{q}| \ll |\boldsymbol{\ell}_1| \sim \mu$, the spectrum arises from the logarithmic $k_\perp$-domain $x|\boldsymbol{q}| \ll |\boldsymbol{k}| \ll \mu$, leading to

$$x\frac{\mathrm{d}I^{(1)}}{\mathrm{d}x} = (2C_R - N_c)\,\frac{\alpha_s}{\pi}\,\frac{L}{\lambda_g}\,\log\left(\frac{\mu^2}{x^2\boldsymbol{q}^2}\right). \tag{2.7}$$

Since $\mu \ll q_\perp$, the dominance of the $k_\perp$-domain $xq_\perp \ll k_\perp \ll \mu$ justifies a posteriori the working assumption $k_\perp \ll q_\perp$. The assumption $t_{\rm f} \gg L$ is also verified, since at fixed x and in the $p^+ \to \infty$ limit, the formation time $t_{\rm f} \sim xp^+/k_\perp^2 \gg xp^+/\mu^2$ is asymptotically large compared to L. This makes the calculation of (2.7) fully self-consistent.

In the limit $L \gg \lambda_g$, all terms of the sum over n in (2.2) become important. The induced spectrum at 'all orders in opacity', corresponding to the case $L \gg \lambda_g$, was derived rigorously in ref. [10] and reads[4]

$$x\frac{\mathrm{d}I}{\mathrm{d}x} = \sum_{n=1}^{\infty} x\frac{\mathrm{d}I^{(n)}}{\mathrm{d}x} = (2C_R - N_c)\,\frac{\alpha_s}{\pi}\,\log\left(\frac{\Delta q_\perp^2(L)}{x^2\boldsymbol{q}^2}\right), \tag{2.8}$$

which in the case of an incoming gluon ($C_R = N_c$) yields the result (2.4). Similarly to the derivation of (2.7), the calculation of (2.8) is fully self-consistent [10]. The working assumptions $k_\perp \ll q_\perp$ and $t_{\rm f} \gg L$ are indeed verified in the dominant $k_\perp$-domain $xq_\perp \ll k_\perp \ll \sqrt{\hat{q}L}$ contributing to (2.8).

To conclude this section, we may recover the parametric dependence of the average radiated energy ΔE found in [10], by integrating the spectrum (2.8) up to x-values where the logarithm in (2.8) is of order unity, setting the limit of validity of the logarithmic approximation. The result is proportional to E and power-suppressed (as $1/q_\perp$) in the hard scale,

$$\Delta E \sim E\int_0^{\mathcal{O}\left(\frac{\Delta q_\perp}{q_\perp}\right)} \mathrm{d}x\, x\frac{\mathrm{d}I}{\mathrm{d}x} \sim (2C_R - N_c)\,\alpha_s\,\frac{\Delta q_\perp(L)}{q_\perp}\,E\,. \tag{2.9}$$

2.2 Physical interpretation

Logarithmic range. At small $x \ll \Delta q_\perp(L)/|\boldsymbol{q}|$ and to logarithmic accuracy, the spectrum (2.8) arises from the region

$$x|\boldsymbol{q}| \ll |\boldsymbol{k}| \ll \Delta q_\perp(L)\,, \tag{2.10}$$

which has a simple physical interpretation.

First, the leftmost inequality is equivalent to saying that at the time $t_{\rm f} \sim \omega/k_\perp^2$ of its emission, the soft gluon does *not* probe the relative displacement $\Delta\vec{r}$ of the *core* charge

[4]The result (2.8) ($L \gg \lambda_g$) could have been guessed from the result (2.7) ($L \ll \lambda_g$) using heuristic arguments. In the case $L \ll \lambda_g$, the prefactor L/λ_g in (2.7) can be interpreted as a (small) rescattering probability. At the same time, μ^2 in the logarithm of (2.7) is the typical transverse exchange (squared) in a single scattering. When $L \gg \lambda_g$, the rescattering probability becomes $1 - \exp(-L/\lambda_g) \simeq 1$, and the typical transverse momentum broadening becomes $\Delta q_\perp^2(L)$.

JHEP01(2015)141

compared to the case of unperturbed (vacuum) propagation. Indeed, denoting v_1 (v_2) the velocity of the incoming (outgoing) energetic charge, the latter statement reads [16]

$$1/\omega \gg \Delta r_\parallel = |v_{2\parallel} - v_{1\parallel}|\, t_{\rm f} \sim \frac{q_\perp^2}{E^2}\frac{\omega}{k_\perp^2} \quad \textit{and} \quad 1/k_\perp \gg \Delta r_\perp = v_{2\perp}\, t_{\rm f} \sim \frac{q_\perp}{E}\frac{\omega}{k_\perp^2}\,, \tag{2.11}$$

which is equivalent to the single condition $k_\perp \gg x q_\perp$.

Second, for the radiation with $k_\perp \gg x q_\perp$ to actually contribute to the *medium-induced* spectrum, the soft gluon should probe the transverse displacement $\Delta r_\perp^{\rm g}$ of the core charge *proper gluon field* induced by rescatterings. This implies $1/k_\perp \ll \Delta r_\perp^{\rm g} \sim (\ell_\perp/\omega)\, t_{\rm f}$, where $\ell_\perp/\omega$ is the deviation angle of the incoming gluon proper field in the medium. This leads to the second inequality of (2.10). In other words, the condition that $k_\perp$ is softer than $\ell_\perp$ is precisely the requirement that the *induced* radiation can be *shaken off* by the additional $\ell_\perp$-kick.

Color factor. The color factor associated to the coherent radiation spectrum (2.8) can also be simply understood. For a general $1 \to 1$ process with incoming and outgoing particles in color representations R and R', respectively, the color factor is $2T_R^a T_{R'}^a$, as can be trivially checked from the structure of the interference terms giving rise to (2.8). Using the identity

$$2T_R^a T_{R'}^a = (T_R^a)^2 + (T_{R'}^a)^2 - (T_R^a - T_{R'}^a)^2 = C_R + C_{R'} - C_t\,, \tag{2.12}$$

where C_t is the color charge exchanged in the t-channel of the hard process, we recover the factor $2C_R - N_c$ in the case (2.8) of asymptotic parton scattering. For the processes $q \to g$ and $g \to q$ mediated by t-channel color triplet exchange, the color factor reads $C_F + N_c - C_F = N_c$, as found in [10].

We emphasize that the calculation of [10] did not use the large N_c limit, and the factor $2C_R - N_c$ in the induced spectrum (2.8) is thus exact and holds for any finite N_c. This factor equals N_c for $g \to g$, and $-1/N_c$ for $q \to q$ forward scattering. In the $N_c \to \infty$ limit, the fully coherent induced radiation associated to $q \to q$ vanishes, which technically arises from the fact that in this case the interference diagrams contributing to (2.8) are non-planar [17]. At finite N_c however, the induced spectrum associated to $q \to q$ is *negative*, which is somewhat unusual,[5] but should not be a source of concern. Indeed, the factor $2C_R - N_c$ in the *induced* (fully coherent) radiation spectrum can be anticipated from the general properties of the *total* radiation spectrum in vacuum,[6] as discussed in ref. [10] and briefly recalled here.

The total spectrum associated to $q \to q$ (or $g \to g$) derived in [10] reads

$$x\frac{{\rm d}I^{\rm vacuum}}{{\rm d}x} \simeq \frac{\alpha_s}{\pi}\left[(2C_R - N_c)\log\left(\frac{x^2\boldsymbol{q}^2}{\Lambda_{\rm IR}^2}\right) + N_c \log\left(\frac{\Lambda_{\rm S}^2}{\Lambda_{\rm IR}^2}\right) + 2N_c \log\left(\frac{\boldsymbol{q}^2}{\Lambda_{\rm IR}\Lambda_{\rm S}}\right)\right]\,, \tag{2.13}$$

[5] Let us mention that there exist other examples, in different kinematic situations and setups, of negative *medium-induced* spectra, see e.g. ref. [18].

[6] We call 'total' spectrum the spectrum at zeroth order in opacity, corresponding to the term ${\rm d}I^{\rm vacuum}$ in (2.2), which is subtracted in the medium-induced spectrum.

JHEP01(2015)141

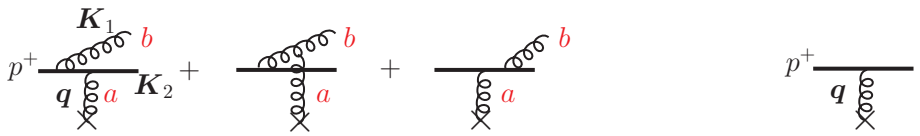

(a) (b)

Figure 3. (a) Amplitude for hard $q \to qg$ production process. (b) Elastic amplitude $\mathcal{M}_{\rm el}$.

where $\Lambda_{\rm IR}$ is an infrared regulator, and $\Lambda_{\rm S}$ a scale satisfying $xq_\perp \ll \Lambda_{\rm S} \ll q_\perp$ but otherwise arbitrary. The first two terms of (2.13) arise from the 'soft' region $k_\perp \leq \Lambda_{\rm S}$, while the last term arises from the 'hard' region $k_\perp \geq \Lambda_{\rm S}$ (the latter extending up to $k_\perp \sim q_\perp$) [10]. When calculating the *medium-induced* radiation spectrum defined in (2.2), nuclear transverse momentum broadening $\Delta q_\perp(L) \sim \ell_\perp$ comes into play, and constrains $k_\perp$ to be soft, $k_\perp < \ell_\perp$, as discussed previously. We thus expect the induced radiation to correspond to the medium-modification of the *soft part* of the total spectrum (2.13), and thus to come with the color factor $2C_R - N_c$. For the $q \to q$ process, we have $2C_F - N_c < 0$ and thus a negative induced spectrum. But this does not contradict any first principle. At the level of the total spectrum (2.13), the fact that $2C_F - N_c < 0$ simply means that the intensity of gluon radiation off a quark into a cone of fixed size ($k_\perp \leq \Lambda_{\rm S}$) *decreases* with increasing $|\boldsymbol{q}|$. At the same time, the *total* radiation intensity, which receives a contribution from gluons with $k_\perp \sim q_\perp$, *increases* with increasing $|\boldsymbol{q}|$ (as expected) with a rate proportional to $(2C_F + N_c)\log|\boldsymbol{q}|$.

3 Forward $q \to qg$ production

We now consider a simple generalization of section 2, by replacing the $1 \to 1$ forward hard process by the $q \to qg$ process, and derive the associated medium-induced soft radiation spectrum.

3.1 Model for $q \to qg$ hard process

The $q \to qg$ production amplitude is depicted in figure 3a, where the final gluon and quark have transverse momenta $\boldsymbol{K}_1 \equiv \vec{K}_{1\perp}$ and $\boldsymbol{K}_2 \equiv \vec{K}_{2\perp}$, and light-cone longitudinal momentum fractions $x_{\rm h} \equiv K_1^+/p^+$ and $1 - x_{\rm h} \equiv K_2^+/p^+$, respectively. We consider the $p^+ \to \infty$ limit at fixed and *finite* $x_{\rm h} \sim \mathcal{O}(1)$. The amplitude of figure 3a is conveniently derived in a light-cone formalism and in light-cone $A^+ = 0$ gauge.

In *scalar* QCD, we find

$$\mathcal{M}_{\rm hard} = \hat{\mathcal{M}}_{\rm el}\cdot 2g(1-x_{\rm h})\cdot\left[T^aT^b\frac{\boldsymbol{K}_1}{\boldsymbol{K}_1^2} + \left[T^b,T^a\right]\frac{\boldsymbol{K}_1-\boldsymbol{q}}{(\boldsymbol{K}_1-\boldsymbol{q})^2} - T^bT^a\frac{\boldsymbol{K}_1-x_{\rm h}\boldsymbol{q}}{(\boldsymbol{K}_1-x_{\rm h}\boldsymbol{q})^2}\right]\cdot\boldsymbol{\varepsilon}_1, \quad (3.1)$$

where $\hat{\mathcal{M}}_{\rm el}$ denotes the Lorentz part (i.e., without color factor) of the elastic amplitude of figure 3b , and $\boldsymbol{\varepsilon}_1 \equiv \vec{\varepsilon}_{1\perp}$ the final gluon physical polarization. Since $\boldsymbol{\varepsilon}_1$ formally disappears after squaring the amplitude and summing over the two physical polarization states, it can be dropped in (3.1).

JHEP01(2015)141

In QCD, the spinor structure makes the amplitude of figure 3a slightly more complicated than (3.1).[7] However, after squaring and summing over polarization states the result for $|\mathcal{M}_{\rm hard}|^2$ in QCD is the same (for a given quark light-cone helicity) *as if* $\mathcal{M}_{\rm hard}$ were given by the scalar QCD expression (3.1), up to the replacement of the overall factor

$$1-x_{\rm h}\ \ \text{(scalar QCD)}\ \ \to\ \ \sqrt{\frac{1+(1-x_{\rm h})^2}{2}}\ \ \text{(QCD)}\,. \tag{3.2}$$

Moreover, specific contributions to $|\mathcal{M}_{\rm hard}|^2$ corresponding to the interference of different graphs of figure 3a (including initial and final state radiation) are reproduced one by one with this replacement. We specially emphasize this fact since only part of these contributions enter the calculation of the induced soft radiation spectrum (see section 3.2).

The overall factor is irrelevant for our purpose, since it will cancel between numerator and denominator in the induced soft radiation spectrum (3.6). We can thus use (in either spinor or scalar QCD):

$$\mathcal{M}_{\rm hard}\ \propto\ T^aT^b\,\frac{\boldsymbol{K}_1}{\boldsymbol{K}_1^2}+\Big[T^b,T^a\Big]\,\frac{\boldsymbol{K}_1-\boldsymbol{q}}{(\boldsymbol{K}_1-\boldsymbol{q})^2}-T^bT^a\,\frac{\boldsymbol{K}_1-x_{\rm h}\boldsymbol{q}}{(\boldsymbol{K}_1-x_{\rm h}\boldsymbol{q})^2}\ . \tag{3.3}$$

We stress that this expression, derived long ago by Gunion and Bertsch [20],[8] holds for any *finite* $x_{\rm h}$ in the $p^+\to\infty$ limit.

The amplitude (3.3) will be our model for the hard process. In addition to $x_{\rm h}\sim\mathcal{O}(1)$, we choose (as in ref. [9]) $\boldsymbol{K}_1$ and $\boldsymbol{K}_2$ to be much larger than the nuclear broadening $\Delta q_\perp$. However, in view of applying the opacity expansion as in the $1\to1$ case studied in section 2, we also choose the dijet *momentum imbalance* $\boldsymbol{q}=\boldsymbol{K}_1+\boldsymbol{K}_2$ to satisfy $|\boldsymbol{q}|\gg\Delta q_\perp$. As a consequence, the dijet imbalance is provided by a single hard exchange $\boldsymbol{q}$ and negligibly affected by soft rescatterings in the medium. In summary we consider the $q\to qg$ process in the kinematics

$$x_{\rm h}\sim\mathcal{O}(1)\qquad\text{and}\qquad|\boldsymbol{K}_1|,\,|\boldsymbol{K}_2|,\,|\boldsymbol{q}|\ \gg\ \Delta q_\perp\,. \tag{3.4}$$

3.2 Medium-induced coherent radiation spectrum

The medium-induced radiation spectrum associated to $q\to qg$ is derived in the *soft* radiation limit defined by

$$x\equiv\frac{k^+}{p^+}\ll1\qquad\text{and}\qquad k_\perp\ \ll\ |\boldsymbol{K}_1|,\,|\boldsymbol{K}_2|,\,|\boldsymbol{q}|\,. \tag{3.5}$$

The calculation is greatly simplified by observing that the hard process structure (3.3) is given by the pictorial rules of figure 2. It is then straightforward to show that the radiation spectrum associated to $q\to qg$ is given, at order n in opacity, by the expression (2.5) with the $1\to1$ replaced by the $q\to qg$ hard process. For instance, at first order in opacity,

$$x\frac{{\rm d}I^{(1)}}{{\rm d}x}\bigg|_{q\to qg}=\frac{\alpha_s}{\pi^2}\int{\rm d}^2\boldsymbol{k}\int\frac{{\rm d}z}{N_c\lambda_g}\int{\rm d}^2\boldsymbol{\ell}\,V(\boldsymbol{\ell})\,\frac{C}{H}\,, \tag{3.6}$$

[7] The QCD calculation can be done using light-cone helicity spinors [19].

[8] In ref. [20], the scalar QCD expression (3.1) is given, but used only in the limit $x_{\rm h}\to0$, where the scalar QCD and spinor QCD expressions of $|\mathcal{M}_{\rm hard}|^2$ coincide (after summing over gluon polarization states).

JHEP01(2015)141

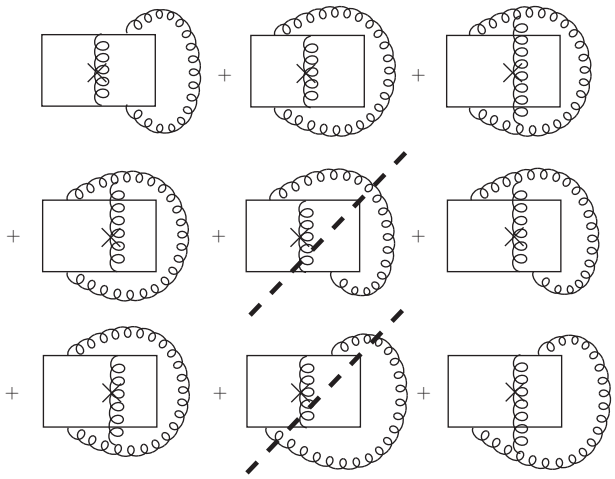

Figure 4. Set H of diagrams corresponding to the $q \to qg$ hard process, appearing in the denominator of the radiation spectrum (3.6). (The barred diagrams are suppressed in the large N_c limit.)

where H is the set of diagrams corresponding to the $q \to qg$ hard process, see figure 4, and C the set of diagrams (to be discussed in detail below) obtained from H by adding one in-medium rescattering and one soft gluon emission. (The diagrams of the set C which will turn out to dominate are shown in figure 5.) In order to simplify the calculation of the set C, we work within the following limits:

(i) We choose the gluon formation time $t_{\rm f}$ to be large not only compared to L (as in section 2) but also compared to the hard process production time $t_{\rm hard}$,

$$t_{\rm f} \sim \frac{k^+}{k_\perp^2} \gg t_{\rm hard} \sim \frac{p^+}{K_{1\perp}^2} \gg L\,. \tag{3.7}$$

For the self-consistency of the derivation, the assumption $t_{\rm f} \gg t_{\rm hard}$ should be checked a posteriori. In other words, the final result (3.16) for the induced radiation spectrum should arise from a kinematical domain where indeed $t_{\rm f} \gg t_{\rm hard}$. As explained in the end of this section, this implies that our derivation is self-consistent provided x belongs to the interval (3.18), which we thus assume in the following.

(ii) We work in the large N_c limit, where non-planar diagrams can be neglected [17]. We stress that the results of ref. [10] for $1 \to 1$ processes, reviewed above in section 2, are independent of this limit and hold for any fixed N_c, as for instance the general rule (2.12) for the color factor of the induced spectrum associated to $1 \to 1$ processes. It is only for $1 \to 2$ processes that we use the $N_c \to \infty$ limit, which greatly simplifies the calculation of the induced spectrum. However, we expect the results for $1 \to 2$ processes to hold beyond this limit, see our comments in the final discussion.

In the limit $t_{\rm f} \gg t_{\rm hard}$, the dominant diagrams of the set C are those where the time of the soft gluon emission vertex, denoted by t in the amplitude or t' in the conjugate amplitude, occurs either long before or long after the interaction vertices of the hard process

JHEP01(2015)141

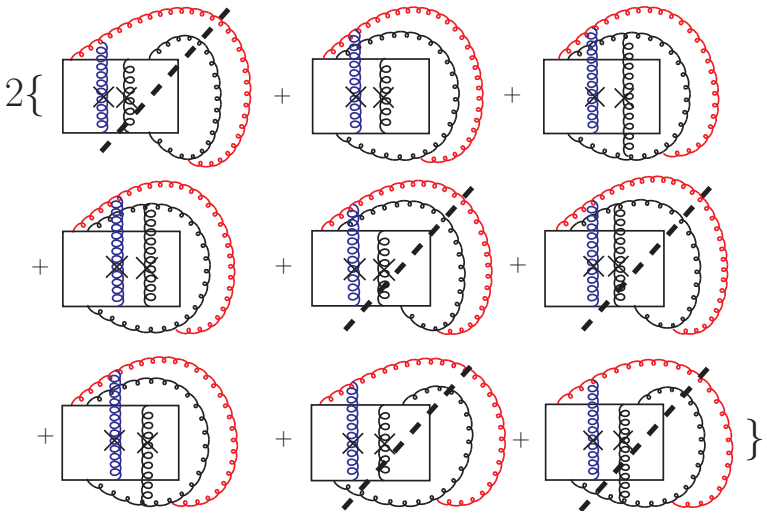

Figure 5. Set C of diagrams (numerator of (3.6)) for the emission of a soft gluon (in red) induced by a single in-medium rescattering (in blue). The black lines of the diagrams stand for the underlying hard $q \to qg$ process depicted in figure 4. For each of the nine graphs above, only one attachment of the rescattering gluon is drawn among all possible ones. Graphs which are suppressed at large N_c (independently of the precise attachment of the rescattering gluon) are barred. See text for details.

shown in figure 4. Similarly to [10], those potentially dominant diagrams can be separated in three classes: purely initial-state radiation (t and t' large and negative), purely final-state radiation (t and t' large and positive), and interference diagrams ($t < 0$ and $t' > 0$, or $t > 0$ and $t' < 0$). As in the case of $1 \to 1$ forward processes, and within the logarithmic accuracy defined in section 2, purely initial-state or purely final-state radiation is suppressed in the medium-induced spectrum. Only interference diagrams remain. The diagrams where the soft gluon is emitted *before* the hard process in the amplitude ($-t \gg t_{\rm hard}$) and *after* in the conjugate amplitude ($t' \gg t_{\rm hard}$) are depicted in figure 5, where the overall factor 2 arises from the contribution of diagrams with $t \gg t_{\rm hard}$ and $-t' \gg t_{\rm hard}$. Note that the diagrams where the soft radiated gluon connects to the final *quark* line are all suppressed in the $N_c \to \infty$ limit, and are thus not drawn in figure 5. Some of the diagrams where the radiated gluon connects to the final hard *gluon* line are also suppressed at large N_c, and are barred in figure 5. Finally, the sum over all possible attachments of the rescattering gluon to the hard quark and gluon lines, as well as to the soft radiated gluon, is implicit in figure 5, where only one of those attachments is drawn.

As already mentioned, the hard process amplitude (3.3) is given by the pictorial rules of figure 2, which allows one to calculate the set H of figure 4 using these rules. Denoting $\boldsymbol{K} = \boldsymbol{K}_1$ we find

$$\begin{aligned} H \,=\, & \left[C_F^2 N_c\right] \cdot \frac{1}{(\boldsymbol{K} - x_{\rm h}\boldsymbol{q})^2} + \left[C_F^2 N_c\right] \cdot \frac{1}{\boldsymbol{K}^2} + \left[C_F N_c^2\right] \cdot \frac{1}{(\boldsymbol{K} - \boldsymbol{q})^2} \\ & + 2 \left\{ \left[-\frac{C_F N_c^2}{2} \right] \cdot \frac{\boldsymbol{K} \cdot (\boldsymbol{K} - \boldsymbol{q})}{\boldsymbol{K}^2 (\boldsymbol{K} - \boldsymbol{q})^2} - \left[\frac{C_F N_c^2}{2} \right] \cdot \frac{(\boldsymbol{K} - \boldsymbol{q}) \cdot (\boldsymbol{K} - x_{\rm h}\boldsymbol{q})}{(\boldsymbol{K} - \boldsymbol{q})^2 (\boldsymbol{K} - x_{\rm h}\boldsymbol{q})^2} \right\} , \end{aligned} \tag{3.8}$$

JHEP01(2015)141

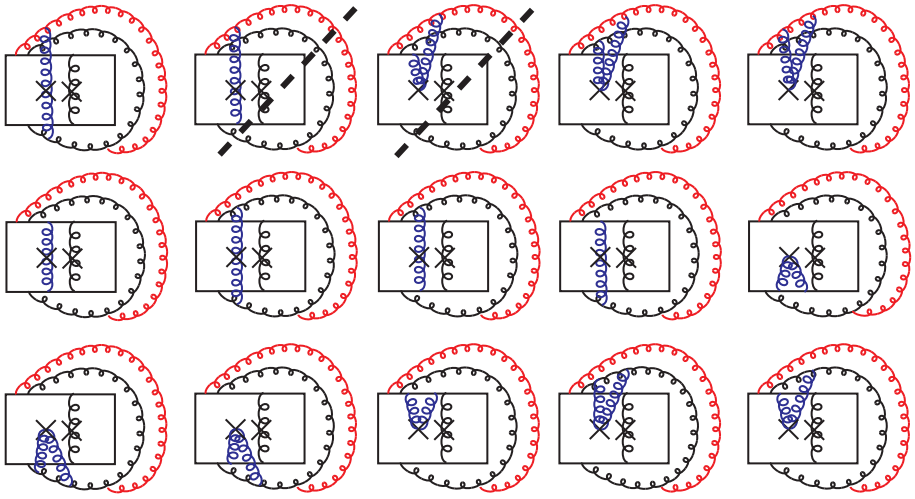

Figure 6. The various attachments of the rescattering gluon (in blue) contributing to the second term of figure 5. Diagrams which are suppressed at large N_c are barred.

where for clarity the color factors arising from the rules of figure 2b are put in between brackets and the explicit factors C_F are kept, despite the fact that $C_F \simeq N_c/2$ at large N_c. The factor 2 in the second line of (3.8) arises from the equality between the second and third lines of figure 4, and the two barred diagrams of figure 4, suppressed at large N_c, have been dropped. Setting now $C_F \to N_c/2$, (3.8) simplifies to

$$H = \frac{N_c^3}{4} \frac{\boldsymbol{q}^2}{\boldsymbol{K}^2(\boldsymbol{K}-\boldsymbol{q})^2} \left[1 + \frac{(1-x_{\rm h})^2 \boldsymbol{K}^2}{(\boldsymbol{K}-x_{\rm h}\boldsymbol{q})^2}\right] . \tag{3.9}$$

The calculation of the set C requires counting all attachments of the rescattering (blue) gluon for each diagram of figure 5. For instance, the second term of figure 5 corresponds to the sum of diagrams depicted in figure 6. In the kinematical limits (3.4) and (3.5), it is easy to check using the rules of figure 2a that for all diagrams of figure 6, the Lorentz factor associated to the hard $q \to qg$ splitting is the same, namely $(\boldsymbol{K}/\boldsymbol{K}^2)\cdot(\boldsymbol{K}/\boldsymbol{K}^2) = 1/\boldsymbol{K}^2$. As for the Lorentz factor associated to the soft radiated (red) gluon, it reads

$$-\frac{\boldsymbol{k}-\frac{x}{x_{\rm h}}\boldsymbol{K}}{(\boldsymbol{k}-\frac{x}{x_{\rm h}}\boldsymbol{K})^2}\cdot\frac{\boldsymbol{k}-\boldsymbol{\ell}}{(\boldsymbol{k}-\boldsymbol{\ell})^2}$$

for the first four diagrams of figure 6 and

$$-\frac{\boldsymbol{k}-\frac{x}{x_{\rm h}}\boldsymbol{K}}{(\boldsymbol{k}-\frac{x}{x_{\rm h}}\boldsymbol{K})^2}\cdot\frac{\boldsymbol{k}}{\boldsymbol{k}^2}$$

for the others. The color factors are calculated using pictorial rules, and we recall that 'virtual contributions', where the rescattering gluon couples to two lines in either the amplitude or conjugate amplitude, contribute a factor (-1), and a symmetry factor $\frac{1}{2}$ when the rescattering gluon connects to the same parton line (see for instance ref. [21]). The diagrams of figure 6 then sum up to ($C_F \simeq N_c/2$):

$$\text{figure 6} \equiv \text{graph 2 of figure 5} = -\frac{1}{\boldsymbol{K}^2}\cdot\frac{\boldsymbol{k}-\frac{x}{x_{\rm h}}\boldsymbol{K}}{(\boldsymbol{k}-\frac{x}{x_{\rm h}}\boldsymbol{K})^2}\cdot\left[\frac{\boldsymbol{k}-\boldsymbol{\ell}}{(\boldsymbol{k}-\boldsymbol{\ell})^2}-\frac{\boldsymbol{k}}{\boldsymbol{k}^2}\right]\frac{N_c^5}{8} . \tag{3.10}$$

JHEP01(2015)141

The other graphs of figure 5 can be similarly calculated, leading to:

$$\text{graph } 3 = -\frac{1}{(\boldsymbol{K}-\boldsymbol{q})^2}\cdot\frac{\boldsymbol{k}-\frac{x}{x_{\rm h}}\boldsymbol{K}}{(\boldsymbol{k}-\frac{x}{x_{\rm h}}\boldsymbol{K})^2}\cdot\left[\frac{\boldsymbol{k}-\boldsymbol{\ell}}{(\boldsymbol{k}-\boldsymbol{\ell})^2}-\frac{\boldsymbol{k}}{\boldsymbol{k}^2}\right]\frac{N_c^5}{8}\,, \tag{3.11}$$

$$\text{graph } 4 = \text{graph } 7 = +\frac{\boldsymbol{K}\cdot(\boldsymbol{K}-\boldsymbol{q})}{\boldsymbol{K}^2(\boldsymbol{K}-\boldsymbol{q})^2}\cdot\frac{\boldsymbol{k}-\frac{x}{x_{\rm h}}\boldsymbol{K}}{(\boldsymbol{k}-\frac{x}{x_{\rm h}}\boldsymbol{K})^2}\cdot\left[\frac{\boldsymbol{k}-\boldsymbol{\ell}}{(\boldsymbol{k}-\boldsymbol{\ell})^2}-\frac{\boldsymbol{k}}{\boldsymbol{k}^2}\right]\frac{N_c^5}{8}\,, \tag{3.12}$$

the other graphs being suppressed at large N_c, as indicated in figure 5. Using (3.10), (3.11) and (3.12), the set C defined by figure 5 (including the overall factor 2) reads

$$C = \frac{N_c^5}{4}\frac{\boldsymbol{q}^2}{\boldsymbol{K}^2(\boldsymbol{K}-\boldsymbol{q})^2}\left[\frac{\boldsymbol{k}-\boldsymbol{\ell}}{(\boldsymbol{k}-\boldsymbol{\ell})^2}-\frac{\boldsymbol{k}}{\boldsymbol{k}^2}\right]\cdot\frac{-(\boldsymbol{k}-\frac{x}{x_{\rm h}}\boldsymbol{K})}{(\boldsymbol{k}-\frac{x}{x_{\rm h}}\boldsymbol{K})^2}\,. \tag{3.13}$$

Finally, inserting (3.9) and (3.13) in (3.6), we find that to logarithmic accuracy, the spectrum arises from the $k_\perp$-domain $x|\boldsymbol{K}| \ll |\boldsymbol{k}| \ll |\boldsymbol{\ell}| \sim \mu$ (recall that $x_{\rm h} \sim \mathcal{O}(1)$) and reads

$$x\frac{{\rm d}I^{(1)}}{{\rm d}x}\bigg|_{q\to qg} = \kappa_{q\to qg}\,\frac{N_c\alpha_s}{\pi}\,\frac{L}{\lambda_g}\,\log\left(\frac{\mu^2}{x^2\boldsymbol{K}^2}\right), \tag{3.14}$$

$$\kappa_{q\to qg} \equiv \frac{(\boldsymbol{K}-x_{\rm h}\boldsymbol{q})^2}{(\boldsymbol{K}-x_{\rm h}\boldsymbol{q})^2+(1-x_{\rm h})^2\boldsymbol{K}^2}\,. \tag{3.15}$$

In the limit $L \gg \lambda_g$, we have performed the calculation of the induced spectrum associated to $q \to qg$ to 'all orders in opacity', using exactly the same procedure as in [10] for $1 \to 1$ processes. A straightforward but somewhat lengthy calculation yields[9]

$$x\frac{{\rm d}I}{{\rm d}x}\bigg|_{q\to qg} = \sum_{n=1}^{\infty} x\frac{{\rm d}I^{(n)}}{{\rm d}x}\bigg|_{q\to qg} = \kappa_{q\to qg}\,\frac{N_c\alpha_s}{\pi}\,\log\left(\frac{\Delta q_\perp^2(L)}{x^2\boldsymbol{K}^2}\right), \tag{3.16}$$

where $\kappa_{q\to qg}$ is defined in (3.15).

To logarithmic accuracy, the radiation spectra associated to the $q \to qg$ and $g \to g$ hard processes, given in (3.16) and (2.8), are proportional to the same logarithm (up to the renaming of the hard scale $\boldsymbol{q} \to \boldsymbol{K}$ in the logarithm of (2.8)), and otherwise differ by the overall factor $\kappa_{q\to qg}$ depending on the kinematical variables defining the $q \to qg$ hard process. In the kinematical situation where $|\boldsymbol{q}| \ll |\boldsymbol{K}|$ and $x_{\rm h} = 1/2$, we recover the factor $\kappa_{q\to qg} = 4/5$ found in ref. [9].

We stress that the result (3.16) arising from the region

$$xK_\perp \ll k_\perp \ll \Delta q_\perp \tag{3.17}$$

was obtained using the assumption (3.7). Our derivation of (3.16) is thus strictly valid provided the condition $t_{\rm f} \gg t_{\rm hard}$, or equivalently $x \gg k_\perp^2/K_\perp^2$, holds in the whole domain (3.17). This implies the following validity range of (3.16),

$$\frac{\Delta q_\perp^2}{K_\perp^2} \ll x \ll \frac{\Delta q_\perp}{K_\perp}\,(\ll 1)\,. \tag{3.18}$$

[9]The difference between the formulae (3.14) and (3.16), corresponding to the cases $L \ll \lambda_g$ and $L \gg \lambda_g$ respectively, can be heuristically understood as in the case of $1 \to 1$ processes, see footnote 4.

JHEP01(2015)141

Let us remark that in ref. [9] the calculation of the spectrum associated to $q \to qg$ (done using a different kinematics, namely, small $|\boldsymbol{q}|$ and $x_{\rm h} = 1/2$ in our notations) does not assume $t_{\rm f} \gg t_{\rm hard}$. Its range of validity is thus broader than the range (3.18) and extends to x-values which are smaller than the lower bound in (3.18). Although not proven in our present study, it is likely that the spectrum (3.16) similarly extends beyond the domain (3.18), for any $|\boldsymbol{q}|$ and $x_{\rm h}$. However keeping track of contributions with $t_{\rm f} \lesssim t_{\rm hard}$ would greatly complicate our calculation.

Finally, we estimate the average radiated energy ΔE associated to (3.16) as was done in (2.9) for the spectrum (2.8),

$$\Delta E|_{q\to qg} \sim E \int_0^{\mathcal{O}\left(\frac{\Delta q_\perp}{K_\perp}\right)} \mathrm{d}x\, x \frac{\mathrm{d}I}{\mathrm{d}x} \sim \kappa_{q\to qg}\, N_c\, \alpha_s\, \frac{\Delta q_\perp(L)}{K_\perp}\, E\,. \tag{3.19}$$

3.3 Interpretation and conjecture

Here we give a simple interpretation of the factor $\kappa_{q\to qg}$ (given in (3.15)), as well as of the color factor N_c appearing in front of the logarithm in (3.16).

For $N_c \geq 3$, the final quark-gluon pair produced in the hard $q \to qg$ process can be in three different irreducible color representations,

$$\mathbf{3} \otimes \mathbf{8} = \mathbf{3} \oplus \bar{\mathbf{6}} \oplus \mathbf{15}\,, \tag{3.20}$$

where the names of the representations indicate their dimensions in the particular case $N_c = 3$. For general N_c the three representations have dimensions

$$K_3 = N_c, \quad K_6 = \frac{N_c(N_c-2)(N_c+1)}{2}, \quad K_{15} = \frac{N_c(N_c+2)(N_c-1)}{2}\,, \tag{3.21}$$

and Casimir operators

$$C_3 = \frac{N_c^2-1}{2N_c}, \quad C_6 = \frac{(N_c-1)(3N_c+1)}{2N_c}, \quad C_{15} = \frac{(N_c+1)(3N_c-1)}{2N_c}\,. \tag{3.22}$$

We observe that the diagrams of figure 5 which are suppressed in the large N_c limit are those where the final qg pair is produced in the fundamental representation $\mathbf{3}$. This is not surprising, since we have seen previously (in the end of section 2.2) that the coherent induced radiation associated to the $q \to q$ process has a color factor $2C_F - N_c = -1/N_c$. Thus, in figure 5 (and in figure 5 only, see the comments below) we may remove from the beginning the 'triplet' component of the final qg pair (or equivalently, project the latter on the $\bar{\mathbf{6}} \oplus \mathbf{15}$ subspace). At large N_c, this is simply achieved by replacing $T^bT^a \to 0$ in (3.3), leaving T^aT^b unchanged. The hard production amplitude with the final quark-gluon triplet component *removed* thus reads

$$\mathcal{M}^{\bar{\mathbf{6}}\oplus\mathbf{15}}_{\rm hard} \;\propto\; T^aT^b \left(\frac{\boldsymbol{K}}{\boldsymbol{K}^2} - \frac{\boldsymbol{K}-\boldsymbol{q}}{(\boldsymbol{K}-\boldsymbol{q})^2}\right)\,. \tag{3.23}$$

JHEP01(2015)141

Squaring this we find

$$|\mathcal{M}^{\bar{\mathbf{6}}\oplus\mathbf{15}}_{\text{hard}}|^2 = \frac{N_c^3}{4}\frac{\boldsymbol{q}^2}{\boldsymbol{K}^2(\boldsymbol{K}-\boldsymbol{q})^2}\,, \tag{3.24}$$

and dividing by the expression (3.9) we get

$$\frac{|\mathcal{M}^{\bar{\mathbf{6}}\oplus\mathbf{15}}_{\text{hard}}|^2}{|\mathcal{M}_{\text{hard}}|^2} = \frac{(\boldsymbol{K}-x_{\text{h}}\boldsymbol{q})^2}{(\boldsymbol{K}-x_{\text{h}}\boldsymbol{q})^2+(1-x_{\text{h}})^2\boldsymbol{K}^2} = \kappa_{q\to qg}\,. \tag{3.25}$$

Thus, the factor $\kappa_{q\to qg}$ is interpreted as the probability that the quark-gluon pair produced in $q\to qg$ is *not* in the 'triplet' color representation.

Thus, the dependence of the spectrum (3.16) on the hard process kinematical variables $\boldsymbol{q}$, $\boldsymbol{K}$, x_{h}, arises from the constraint that at large N_c, only non-triplet qg pairs can contribute to the set C of diagrams (figure 5). This 'selection' of the $\bar{\mathbf{6}}\oplus\mathbf{15}$ subspace is due to the specific connection of the soft radiated gluon between initial and final state in figure 5. In particular, it would be incorrect to attribute this effect to the smaller dimension $K_3 = N_c$ of the triplet representation as compared to the dimension of the $\bar{\mathbf{6}}\oplus\mathbf{15}$ subspace ($K_6+K_{15}=N_c^3$ at large N_c). For instance, the lower dimension of $\mathbf{3}$ does not prevent the qg pair to be produced as a triplet in the hard $q\to qg$ process (see set H of diagrams, figure 4), even at large N_c.

The logarithmic range (3.17) can be interpreted in a similar way as the range (2.10) for $1\to 1$ processes (see section 2.2). Moreover, in the present $q\to qg$ case, the condition $xK_\perp \ll k_\perp$ written as $1/k_\perp \gg \Delta r_\perp \sim v_\perp\, t_{\text{f}} \sim (K_\perp/E)\cdot(\omega/k_\perp^2)$ (similarly to (2.11)) means that at the time of its emission, the radiated gluon does not probe the transverse size $\Delta r_\perp$ of the qg pair. From the point of view of soft radiation, the qg pair thus behaves as an effectively pointlike system.

Finally, the color factor N_c in (3.16) can be simply understood from the rule (2.12). Indeed, since coherent radiation arises from a kinematical domain where the qg pair is effectively pointlike, the result should depend on its *total* color charge, not on the color of its separate constituents. Since the color state of the final qg pair in figure 5 is either $\bar{\mathbf{6}}$ or $\mathbf{15}$, and these two representations have the same Casimir operator at large N_c, namely $3N_c/2$, the rule (2.12) gives ($R'=\bar{\mathbf{6}}$ or $\mathbf{15}$)

$$2T^a_{\mathbf{3}}T^a_{R'} = C_{\mathbf{3}} + C_{R'} - C_{\mathbf{8}} = \frac{N_c}{2}+\frac{3N_c}{2}-N_c = N_c\,. \tag{3.26}$$

A conjecture. Guided by the above interpretation of our result, we conjecture the following simple formula for the medium-induced radiation spectrum associated to hard forward $1\to n$ processes (where the n final-state partons have finite longitudinal momentum fractions $x_i = K_i^+/p^+ \sim \mathcal{O}(1)$ and transverse momenta $\boldsymbol{K}_i$ of similar magnitude $\sim|\boldsymbol{K}|$),

$$x\frac{\mathrm{d}I}{\mathrm{d}x}\bigg|_{1\to n} = \left[\sum_{R'} P_{R'}(C_R + C_{R'} - C_t)\right]\frac{\alpha_s}{\pi}\,\log\left(\frac{\Delta q_\perp^2(L)}{x^2\boldsymbol{K}^2}\right), \tag{3.27}$$

with C_R and C_t the color charges of the incoming parton and of the t-channel exchange, and $P_{R'}$ the probability for the (effectively pointlike) n-parton state to be produced in the

JHEP01(2015)141

color representation R' in the hard process. ($P_{R'}$ may depend on the kinematical variables x_i, $\boldsymbol{K}_i$ defining the hard $1 \to n$ process, as in the $q \to qg$ case.)

As a first illustration, the spectrum associated to $g \to q\bar{q}$ derived in ref. [9] can be obtained from (3.27) by setting $P_{R'} = P_{\mathbf{8}} = 1$ (at large N_c the final $q\bar{q}$ is color octet with unit probability) and $C_R = C_{R'} = C_t = N_c$. Not surprisingly, since the final $q\bar{q}$ is effectively pointlike, the result is the same as for the $g \to g$ process considered in refs. [5, 10].

As a second example, let us mention that we explicitly verified (3.27) in the case of the $g \to gg$ process. Using the same theoretical setup (including the large N_c limit) and following the same procedure as for the $q \to qg$ process, we find an expression for the radiation spectrum similar to (3.16), but with a different overall factor κ,

$$x \frac{\mathrm{d}I}{\mathrm{d}x}\bigg|_{g\to gg} = \kappa_{g\to gg} \, \frac{N_c \alpha_s}{\pi} \, \log\left(\frac{\Delta q_\perp^2(L)}{x^2 \boldsymbol{K}^2}\right), \tag{3.28}$$

$$\kappa_{g\to gg} \equiv 1 + \frac{(\boldsymbol{K} - x_{\mathrm{h}}\boldsymbol{q})^2}{(\boldsymbol{K} - x_{\mathrm{h}}\boldsymbol{q})^2 + x_{\mathrm{h}}^2(\boldsymbol{K} - \boldsymbol{q})^2 + (1 - x_{\mathrm{h}})^2 \boldsymbol{K}^2}\,. \tag{3.29}$$

(Note that $\kappa_{g\to gg} = 5/3$ when $|\boldsymbol{q}| \ll |\boldsymbol{K}|$ and $x_{\mathrm{h}} = 1/2$.) To check whether (3.28), (3.29) coincide with (3.27), we must sum in (3.27) over the different representations R' of the final gg pair. At large N_c, a two-gluon system can be in six color representations [22],

$$\mathbf{8} \otimes \mathbf{8} = \mathbf{8_a} \oplus \mathbf{10} \oplus \mathbf{1} \oplus \mathbf{8_s} \oplus \mathbf{27} \oplus \mathbf{0}\,, \tag{3.30}$$

where as in (3.20) the representations are labelled according to their dimensions in the case $N_c = 3$. In particular $\mathbf{0}$ is a symmetric representation which is absent when $N_c = 3$. For $N_c > 3$ the representations appearing in the r.h.s. of (3.30) have the Casimir operators N_c, $2N_c$, 0, N_c, $2(N_c + 1)$ and $2(N_c - 1)$, respectively [22]. Thus, at large N_c the bracket in (3.27) reads

$$\sum_{R'} P_{R'}(C_R + C_{R'} - C_t) = \sum_{R'} P_{R'}\, C_{R'} = (2 - P_{\mathbf{8_a}} - P_{\mathbf{8_s}})\, N_c\,, \tag{3.31}$$

where we used $C_R = C_t = N_c$, probability conservation $\sum_{R'} P_{R'} = 1$, and the fact that the probability $P_{\mathbf{1}}$ for the final gg pair to be color singlet is suppressed at large N_c. The probability $P_{\mathbf{8}} \equiv P_{\mathbf{8_a}} + P_{\mathbf{8_s}}$ to produce a *color octet* gg pair can be simply evaluated using pictorial rules for the projection operators on specific color representations [22]. Analogously to what was done in (3.25) the calculation gives

$$P_{\mathbf{8}} = \frac{|\mathcal{M}^{\mathbf{8_a}}_{g\to gg}|^2 + |\mathcal{M}^{\mathbf{8_s}}_{g\to gg}|^2}{|\mathcal{M}_{g\to gg}|^2} = \frac{x_{\mathrm{h}}^2(\boldsymbol{K} - \boldsymbol{q})^2 + (1 - x_{\mathrm{h}})^2 \boldsymbol{K}^2}{(\boldsymbol{K} - x_{\mathrm{h}}\boldsymbol{q})^2 + x_{\mathrm{h}}^2(\boldsymbol{K} - \boldsymbol{q})^2 + (1 - x_{\mathrm{h}})^2 \boldsymbol{K}^2}\,. \tag{3.32}$$

Plugging (3.32) in (3.31), we see that the expression (3.27) reproduces eqs. (3.28), (3.29). This completes the check of the conjectured expression (3.27) in the case of the $g \to gg$ process.

We conclude by a few remarks on the expected validity range of the conjecture (3.27).

First, we recall that the result (3.16) (and similarly (3.28)) has been derived within the limit (3.7), resulting in the validity range (3.18). As mentioned in the end of section 3.2,

JHEP01(2015)141

there are indications from the calculations in the dipole formalism of ref. [9] that the expression for the spectrum may be valid also for x below the lower bound of (3.18). We expect the same for the induced spectrum associated to $1 \to n$ forward processes conjectured in (3.27).

Second, in order to perform the calculation of the induced spectrum associated to $q \to qg$ (and $g \to gg$), we used $N_c \gg 1$ as a simplifying theoretical limit. We however expect the conjecture (3.27) to hold for any N_c. Indeed, the induced radiation associated to $q \to qg$ 'sees' the final qg system as a compact object (*within logarithmic accuracy*), which makes the spectrum expressible as a sum of spectra associated to $1 \to 1$ processes. Using the fact that the color factor $C_R + C_{R'} - C_t$ associated to a general $1 \to 1$ process (see (2.12)) holds for any N_c (as recalled in section 2.2), it seems clear that (3.27) should hold beyond the large N_c limit.

Finally, we expect the conjecture (3.27) to fail beyond logarithmic accuracy, since in this case the final partonic system does not act as a pointlike object any longer.

4 Comments on nuclear suppression phenomenology

4.1 Nuclear attenuation factor

As mentioned in section 2.1 (see paragraph after (2.2)), the definition of the medium-induced spectrum (2.1) we have used corresponds to the conditional probability to have soft gluon emission provided a dijet (or more generally n-jet) with specific kinematics is produced. We stress that a sum over the possible dijet color states is performed in both the numerator and denominator of (2.1). This is also apparent from (3.27), which can be formally rewritten as

$$\mathrm{d}I|_{1\to n} = \sum_{R'} P_{R'} \cdot \mathrm{d}I^{R'} = \sum_{R'} \frac{\mathrm{d}\sigma^{R'}_{\mathrm{prod}}}{\sum_{R''} \mathrm{d}\sigma^{R''}_{\mathrm{prod}}} \cdot \frac{\mathrm{d}\sigma^{R'}_{\mathrm{rad}}}{\mathrm{d}\sigma^{R'}_{\mathrm{prod}}} = \frac{\sum_{R'} \mathrm{d}\sigma^{R'}_{\mathrm{rad}}}{\sum_{R'} \mathrm{d}\sigma^{R'}_{\mathrm{prod}}}\,, \tag{4.1}$$

where $\mathrm{d}I^{R'}$ denotes the induced spectrum associated to dijet production in the color representation R',

$$x\frac{\mathrm{d}I^{R'}}{\mathrm{d}x} \equiv (C_R + C_{R'} - C_t)\,\frac{\alpha_s}{\pi}\,\log\left(\frac{\Delta q_\perp^2(L)}{x^2 \boldsymbol{K}^2}\right). \tag{4.2}$$

Due to the color representation dependence of (4.2) the induced spectrum defined by (2.1) cannot be directly interpreted in terms of induced energy loss applied to the phenomenology of nuclear suppression in p–A collisions. However, the step towards phenomenology is quite straightforward. The dijet nuclear attenuation factor R_{pA} provided by the experiment depends on p–p and p–A dijet cross sections implicitly summed over all color representations R' of the dijet,

$$R_{\mathrm{pA}} \equiv \frac{1}{A}\frac{\mathrm{d}\sigma_{\mathrm{pA}}}{\mathrm{d}\sigma_{\mathrm{pp}}} = \frac{1}{A}\frac{\sum_{R'} \mathrm{d}\sigma^{R'}_{\mathrm{pA}}}{\sum_{R''} \mathrm{d}\sigma^{R''}_{\mathrm{pp}}} = \sum_{R'} \frac{\mathrm{d}\sigma^{R'}_{\mathrm{pp}}}{\sum_{R''} \mathrm{d}\sigma^{R''}_{\mathrm{pp}}} \cdot \frac{\frac{1}{A}\mathrm{d}\sigma^{R'}_{\mathrm{pA}}}{\mathrm{d}\sigma^{R'}_{\mathrm{pp}}} = \sum_{R'} P_{R'}\, R^{R'}_{\mathrm{pA}}\,. \tag{4.3}$$

Here we used $P_{R'} = \mathrm{d}\sigma^{R'}_{\mathrm{pp}}/(\sum_{R''} \mathrm{d}\sigma^{R''}_{\mathrm{pp}})$. Thus, R_{pA} can be obtained by first calculating the attenuation factors $R^{R'}_{\mathrm{pA}}$ separately for each of the color states R' and then averaging over R' with the probabilities $P_{R'}$.

JHEP01(2015)141

4.2 Dynamical color filtering

In our setup, the final compact partonic configurations are all the more suppressed that their color charge $C_{R'}$ is large, see (4.2). This resembles the *color filtering* idea of Brodsky and Hoyer [23], where at sufficiently large $x_{\rm F}$ only compact *color singlet* partonic states can emerge from the nucleus, however with one important distinction. The color singlet partonic states considered in ref. [23] are already present in the Fock expansion of the incoming hadron wave function, and filtered by the target nucleus into the final state due to their low interaction probability. In our setup, the outgoing n-parton system is produced in the hard process, and may belong to a different color representation from that of the projectile parton, the color charge difference arising from the color exchange in the t-channel of the hard production process.

The r.h.s. of (4.3) can thus be viewed as a generalization of the color filtering idea, which might be named *dynamical* color filtering: different color states *produced in the hard process* emerge with different nuclear suppressions, which enter the overall nuclear modification factor being weighed by the associated probabilities. In general the nucleus will filter out the color state of smallest charge $C_{R'}$, corresponding to minimal energy loss.

The dependence of fully coherent induced radiation on the color charge should have simple consequences in phenomenology, as illustrated by the following example. Suppose some part of the phase space for dijet forward production is dominated by the $qg \to qg$ subprocess in the center-of-mass frame (corresponding to $q \to qg$ process in the target rest frame). Then, according to (4.3) the nuclear suppression factor due to coherent induced radiation will be limited *from below* by the probability for the final qg dijet to be in the fundamental representation for which the induced radiation is suppressed. A similar effect is expected for *single* jet (or hadron) hadroproduction in p–A collisions at forward rapidities and sufficiently high transverse momenta, since the cross section of the latter process is derived from the integrated production cross section of back-to-back jets.

Acknowledgments

S.P. would like to thank Tseh Liou and Al Mueller for a rich and instructive correspondence, which motivated the present study. We also thank François Arleo for useful discussions and comments on the manuscript. Feynman diagrams have been drawn with the JaxoDraw software [24]. This work is funded by "Agence Nationale de la Recherche" under grant ANR-PARTONPROP.

References

[1] D. d'Enterria, *Landolt-Börnstein. Vol. 1-23A: Jet quenching*, Springer Verlag, Heidelberg Germany (2009) [arXiv:0902.2011] [INSPIRE].

JHEP01(2015)141

[2] I. Vitev, *Non-Abelian energy loss in cold nuclear matter*, *Phys. Rev.* **C 75** (2007) 064906 [hep-ph/0703002] [INSPIRE].

[3] R.B. Neufeld, I. Vitev and B.-W. Zhang, *A possible determination of the quark radiation length in cold nuclear matter*, *Phys. Lett.* **B 704** (2011) 590 [arXiv:1010.3708] [INSPIRE].

[4] H. Xing, Y. Guo, E. Wang and X.-N. Wang, *Parton Energy Loss and Modified Beam Quark Distribution Functions in Drell-Yan Process in p+A Collisions*, *Nucl. Phys.* **A 879** (2012) 77 [arXiv:1110.1903] [INSPIRE].

[5] F. Arleo, S. Peigné and T. Sami, *Revisiting scaling properties of medium-induced gluon radiation*, *Phys. Rev.* **D 83** (2011) 114036 [arXiv:1006.0818] [INSPIRE].

[6] F. Arleo and S. Peigné, *J/ψ suppression in p-A collisions from parton energy loss in cold QCD matter*, *Phys. Rev. Lett.* **109** (2012) 122301 [arXiv:1204.4609] [INSPIRE].

[7] F. Arleo and S. Peigné, *Heavy-quarkonium suppression in p-A collisions from parton energy loss in cold QCD matter*, *JHEP* **03** (2013) 122 [arXiv:1212.0434] [INSPIRE].

[8] F. Arleo, R. Kolevatov, S. Peigné and M. Rustamova, *Centrality and $p_\perp$ dependence of J/ψ suppression in proton-nucleus collisions from parton energy loss*, *JHEP* **05** (2013) 155 [arXiv:1304.0901] [INSPIRE].

[9] T. Liou and A.H. Mueller, *Parton energy loss in high energy hard forward processes in proton-nucleus collisions*, *Phys. Rev.* **D 89** (2014) 074026 [arXiv:1402.1647] [INSPIRE].

[10] S. Peigné, F. Arleo and R. Kolevatov, *Medium-induced gluon radiation: an update*, arXiv:1402.1671 [INSPIRE].

[11] G. Ovanesyan and I. Vitev, *An effective theory for jet propagation in dense QCD matter: jet broadening and medium-induced bremsstrahlung*, *JHEP* **06** (2011) 080 [arXiv:1103.1074] [INSPIRE].

[12] M. Gyulassy, P. Lévai and I. Vitev, *Reaction operator approach to nonAbelian energy loss*, *Nucl. Phys.* **B 594** (2001) 371 [nucl-th/0006010] [INSPIRE].

[13] R. Baier, Y.L. Dokshitzer, A.H. Mueller, S. Peigné and D. Schiff, *Radiative energy loss and p_T broadening of high-energy partons in nuclei*, *Nucl. Phys.* **B 484** (1997) 265 [hep-ph/9608322] [INSPIRE].

[14] Y.L. Dokshitzer, *Perturbative QCD (and beyond)*, in *Lectures on QCD*, F. Lenz et al. eds., Springer-Verlag, Heidelberg Germany (1997), pg. 87.

[15] R. Baier, Y.L. Dokshitzer, A.H. Mueller, S. Peigné and D. Schiff, *Radiative energy loss of high-energy quarks and gluons in a finite volume quark-gluon plasma*, *Nucl. Phys.* **B 483** (1997) 291 [hep-ph/9607355] [INSPIRE].

[16] Y.L. Dokshitzer, *Perturbative QCD for beginners*, in *Proceedings of European School of High-Energy Physics*, Dubna Russia (1995), pg. 59.

[17] G. 't Hooft, *A Planar Diagram Theory for Strong Interactions*, *Nucl. Phys.* **B 72** (1974) 461 [INSPIRE].

[18] U.A. Wiedemann, *Jet quenching versus jet enhancement: A Quantitative study of the BDMPS-Z gluon radiation spectrum*, *Nucl. Phys.* **A 690** (2001) 731 [hep-ph/0008241] [INSPIRE].

[19] G.P. Lepage and S.J. Brodsky, *Exclusive Processes in Perturbative Quantum Chromodynamics*, *Phys. Rev.* **D 22** (1980) 2157 [INSPIRE].

JHEP01(2015)141

[20] J.F. Gunion and G. Bertsch, *Hadronization by color bremsstrahlung*, *Phys. Rev.* **D 25** (1982) 746 [INSPIRE].

[21] R. Baier, Y.L. Dokshitzer, A.H. Mueller and D. Schiff, *Medium induced radiative energy loss: Equivalence between the BDMPS and Zakharov formalisms*, *Nucl. Phys.* **B 531** (1998) 403 [hep-ph/9804212] [INSPIRE].

[22] Y. Dokshitzer and G. Marchesini, *Hadron collisions and the fifth form-factor*, *Phys. Lett.* **B 631** (2005) 118 [hep-ph/0508130] [INSPIRE].

[23] S.J. Brodsky and P. Hoyer, *The Nucleus as a Color Filter in QCD Decays: Hadroproduction in Nuclei*, *Phys. Rev. Lett.* **63** (1989) 1566 [INSPIRE].

[24] D. Binosi, J. Collins, C. Kaufhold and L. Theussl, *JaxoDraw: A Graphical user interface for drawing Feynman diagrams. Version 2.0 release notes*, *Comput. Phys. Commun.* **180** (2009) 1709 [arXiv:0811.4113] [INSPIRE].

JHEP01(2015)141